Clin Neuroradiol (2019) 29:595–604
https://doi.org/10.1007/s00062-018-0704-2

ORIGINALPAPER

MRI Phenotype of *RELA*-fused Pediatric Supratentorial Ependymoma

Johannes Nowak[1,2] · Stephanie Theresa Jünger[3] · Henner Huflage[2] · Carolin Seidel[1] · Annika Hohm[1] · Lindsey A. Vandergrift[4] · Katja von Hoff[5] · Stefan Rutkowski[5] · Torsten Pietsch[3] · Monika Warmuth-Metz[1]

Received: 27 March 2018 / Accepted: 22 June 2018 / Published online: 19 July 2018

Abstract

Purpose Epigenetic profiling has recently identified clinically and molecularly distinct subgroups of ependymoma. The 2016 World Health Organization (WHO) classification recognized supratentorial ependymomas (ST-EPN) with REL-associated protein/p65 (RELA) fusion as a clinicopathological entity. These tumors represent 70% of pediatric ST-EPN characterized by recurrent *C11orf95-RELA* fusion transcripts, which lead to pathological activation of the nuclear factor 'kappa-light-chain-enhancer' of activated B-cells (NF-κB) signaling pathway. Cyclin-dependent kinase inhibitor 2A (*CDKN2A*) inactivation has also been reported to correlate with poor prognosis. Here, we systematically describe magnetic resonance imaging (MRI) characteristics of *RELA*-fused ST-EPN, with respect to *CDKN2A* deletion status.

Methods Our cohort of patients with ST-EPN ($n=57$) was obtained from the database of the German Brain Tumor Reference Center of the German Society for Neuropathology and Neuroanatomy (DGNN), and tumors were diagnosed according to the 2016 WHO classification. Molecular characterization identified 47 *RELA*-fused tumors. We analyzed the preoperative MRI according to standardized criteria, and comparison was performed between *CDKN2A* altered ($n=21$) and *CDKN2A* wild type ($n=26$) tumors.

Results The *RELA*-fused ST-EPN showed a spectrum of predominantly hemispheric tumors with cysts and necrosis. Statistical analysis on *CDKN2A* status revealed significant differences in terms of younger manifestation age ($p=0.002$) and more intratumoral hemorrhage in T2-weighted imaging (T2WI) ($p=0.010$) in wild type tumors; however, the location was not a parameter for differentiation.

Conclusion This study first provides comprehensive MRI data for *RELA*-fused ST-EPN as a distinct entity, with further interest on *CDKN2A* genomic status. Patient stratification by morphological MRI alone seems difficult at present. The results may support ongoing research in ST-EPN within the framework of the radiogenomics concept.

Keywords Supratentorial ependymoma · Magnetic resonance imaging · Radiogenomics · RELA fusion · CDKN2A deletion

Electronic supplementary material The online version of this article (https://doi.org/10.1007/s00062-018-0704-2) contains supplementary material, which is available to authorized users.

✉ Johannes Nowak
Nowak_J1@ukw.de

[1] Reference Center for Neuroradiology, Institute for Diagnostic and Interventional Neuroradiology, University Hospital of Würzburg, Josef-Schneider-Str. 11, 97080 Würzburg, Germany

[2] Department of Diagnostic and Interventional Radiology, University Hospital of Würzburg, Oberdürrbacher Str. 6, 97080 Würzburg, Germany

[3] Department of Neuropathology, Brain Tumor Reference Center of the DGNN, University of Bonn, Sigmund-Freud-Str. 25, 53127 Bonn, Germany

[4] Departments of Radiology and Pathology, Massachusetts General Hospital, Harvard Medical School, 149 Thirteenth St, Charlestown, MA 02129, USA

[5] Department of Pediatric Hematology and Oncology, University Medical Center Hamburg-Eppendorf, Martinistr. 52, 20246 Hamburg, Germany

Introduction

Ependymomas (EPN) are glial brain tumors that can arise in all compartments of the central nervous system (CNS) and account for approximately 12% of all pediatric intracranial tumors [1, 2]. To date, complete resection followed by radiotherapy remains the only curative therapeutic option for most EPN. Local tumor progression and metastatic disease are the main clinical challenges. Novel strategies to improve the overall prognosis, while simultaneously reducing severe long-term morbidity, have to consider that EPN in different compartments represent distinct disease entities [3].

Recently, molecular biomarkers have become essential to classify CNS tumors and to stratify affected patients. In 2014, recurrent *C11orf95-RELA* gene fusions were identified in more than 70% of pediatric supratentorial ependymomas (ST-EPN), leading to pathological activation of proinflammatory and oncogenic nuclear factor kappa B (NF-κB) signaling. Recent data indicate that *RELA*(REL-associated protein/p65)-fused tumors are connected with an unfavorable outcome among pediatric ST-EPN [4]. Thus, *RELA*-fused ST-EPN have been defined as a novel disease entity by the revised 2016 WHO classification of tumors of the CNS [5]. Additionally, it has been shown that p14/ARF downregulation, frequently caused by cyclin-dependent kinase inhibitor 2A (*CDKN2A*) deletion or hypermethylation, is associated with biologically aggressive EPN and p53 accumulation [6]. Pajtler et al. show that homozygous *CDKN2A* deletions occur exclusively in *RELA*-fused ST-EPN [3] and *CDKN2A* deletion was also associated with dismal prognosis in several retrospective cohorts [7–9].

From the imaging perspective, diagnostic interpretation of magnetic resonance imaging (MRI) studies was for a long time primarily related to histopathological features. Promising results have been published regarding recent advances in genotyping of CNS tumors (e.g. different molecular subgroups in glioblastoma and medulloblastoma) and correlation with the MRI phenotype based on the "radiogenomics" concept [10–12]. There are currently no detailed data available regarding MRI features of the newly identified *RELA*-fused ST-EPN entity, and to what extent *CDKN2A* alterations result in a distinct MRI phenotype. A current consensus paper, however, states that molecular analysis and central radiological review should be part of all future clinical trials in ST-EPN [13]. It can be hypothesized that the dismal prognosis due to *RELA* fusion and *CDKN2A* deletion may be reflected by an aggressive MRI phenotype (e.g. necrosis, hemorrhage, diffusion restriction). In this study a detailed overview of MRI morphology in *RELA*-fused ST-EPN is provided and MRI characteristics dependent on *CDKN2A* genomic status are compared.

Methods

Study Population

A total of 57 patients with the neuropathological diagnosis of ST-EPN of WHO grades II and III and known molecular characteristics (regarding *RELA* fusion and *CDKN2A* alteration status) were identified at the German Brain Tumor Reference Center of the German Society for Neuropathology and Neuroanatomy (DGNN) and corresponding MRI studies were then obtained from the brain tumor database of the Neuroradiological Reference Center for Pediatric Brain Tumors. Patients were diagnosed with ST-EPN from 2001–2011 and registered in the HIT2000 and HIT-MED (ClinicalTrials.gov/NCT00303810) studies. All procedures were approved by the local and central ethics review boards of the HIT studies and performed in accordance with the Helsinki Declaration of the World Medical Association.

Molecular Analysis

Analysis of *RELA* fusion status was performed at the Brain Tumor Reference Center in Bonn, Germany, as described previously [14, 15]. For nuclear RelA protein expression, immunohistochemical (IHC) staining of formalin-fixed paraffin-embedded (FFPE) samples was performed using anti-NF-κB p65 rabbit antibody D14E12 (1:400 Cell Signaling Technology, Danvers, MA, USA). A sufficient quantity of mRNA was available in 15 samples, and *C11orf95-RELA* were confirmed on the RNA level as described in [20, 21] by RT-PCR and subsequent sequencing. The *CDKN2A* genomic status was determined by molecular inversion probe analysis as described previously [16, 17]. Loss of p16 protein (indicating homozygous *CDKN2A* deletion) was analyzed by IHC on paraffin-embedded tumor samples using anti-p16 monoclonal mouse antibody (anti-$p16^{INK4a}$ (E6H4), Ventana-Roche, Mannheim, Germany).

Image Analysis

The MRI data were generated at local centers with MRI scanners of different manufacturers at 1.0–3.0 T field strength. The MRI datasets included non-enhanced T1-weighted images (T1WI), T2-weigted images (T2WI), T2* or susceptiblity-weighted images (SWI), diffusion-weighted images (DWI), and contrast-enhanced T1WI in at least one plane. When datasets were incomplete the available sequences were analyzed. A retrospective view of all MRI scans was performed by two neuroradiologists (M.W.-M. and J.N.) in consensus. We applied standardized MRI criteria, adapted from the routine image evaluation of the Neuroradiological Reference Center. Tumor diameters were measured in three orthogonal dimensions (along the

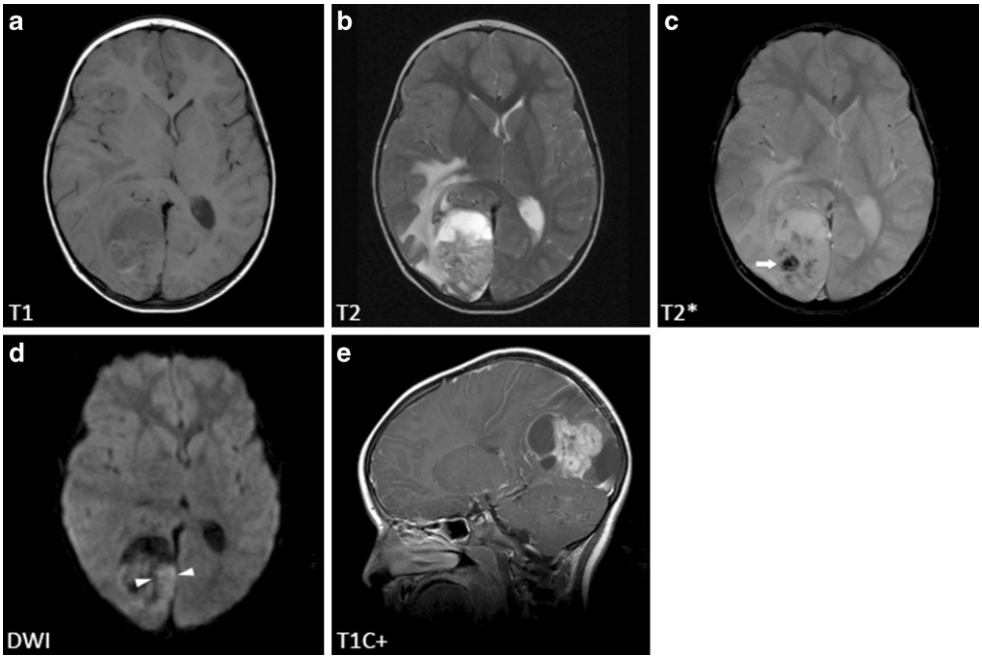

Fig. 1 Typical imaging findings in *RELA*-fused ST-EPN (**a**–**e** Siemens Vision 1.5 T). The MR images show inhomogeneous signal in T1 and T2 (**a,b**) as well as peritumoral edema (**b**), signs of intratumoral hemorrhage (*white arrow* in **c**), restricted diffusion (*arrowheads* in **d**) and strong contrast enhancement (**e**)

axial, coronal and sagittal axes, in cm), and tumor volume was then calculated according to a common approximation formula ($a \times b \times c \times 0.5$ cm^3). Tumor location was assigned based on the following categories: frontal, parietal, temporal, occipital and intraventricular. T1 and T2-signal intensities of the tumor were defined in relation to that of the cortex. We further analyzed the presence of cysts within the tumor, cyst localization (peripheral or other) and signal of cysts (isointense/hyperintense compared to CSF or mixed). Predominant morphology was defined as solid, cystic or necrotic (when >50% of the tumor volume). The homogeneity of the solid tumor (in T1WI and T2WI) and the delineation of the tumor from the adjacent brain tissue (well-defined or ill-defined borders) were evaluated. Possible hydrocephalus or peritumoral edema as well as the maximum extent of edema (in cm, measured in axial plane) were registered. Another parameter was the pattern of contrast (gadolinium) enhancement within the tumors (intensity, percentage of enhancing solid volume, homogeneity), as well as the presence or lack of diffusion restriction in DWI. After consideration of all available sequences, we determined whether intratumoral hemorrhage was present. When provided by the external referring centers, computed tomography (CT) scans were also considered, with a focus on the presence of hemorrhage and tumor calcification.

Statistical Analysis

After analysis and encoding of imaging parameters in *RELA*-fused ST-EPN (for either numerical or categorical variables), comparison was performed between tumors with

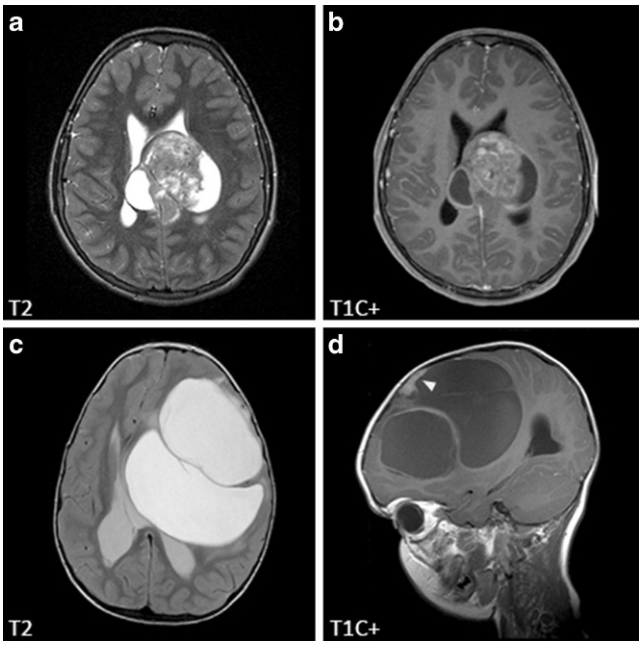

Fig. 2 The MR images in (**a**) and (**b**) demonstrate a *RELA*-fused ST-EPN with solid components and smaller cystic portions in the tumor periphery (Siemens Avanto 1.5 T). In contrast, the *RELA*-fused ST-EPN (**c,d** Siemens Symphony 1.5 T) is predominantly cystic with only small solid parts (**d**, *arrowhead*). Note that all tumors of our cohort showed some solid, enhancing areas to varying extents

(*CDKN2A* deleted) and without *CDKN2A* deletion (wild type = *CDKN2A* WT), in order to test for differences between these groups. For numerical variables, the Shapiro-Wilk test was performed to test for normal distribution. A t-test was used for normally distributed variables and a Mann-Whitney U-test when values were not normally

Table 1 Overview of patient and imaging data in *RELA*-fused ST-EPN, and comparison of *CDKN2A* deleted vs. *CDKN2A* wild type tumors

		RELA-fused $n = 47$		Comparison				*p*-value
				CDKN2A WT $n = 26$		*CDKN2A* del $n = 21$		
		n	%	*n*	%	*n*	%	
Gender		47		26		21		0.774
	Male	24	*51.06*	13	*50.00*	11	*52.38*	
	Female	23	*48.94*	13	*50.00*	10	*47.62*	
Age at diagnosis (years)	Median	6.36		4.46		10.12		**0.002**
	Mean	7.89		5.84		10.57		
	SD	5.16		4.45		4.78		
CDKN2A genomic status		47		26		21		
	CDKN2A WT	26	*55.32*	26	*100.00*			
	CDKN2A deleted	21	*44.68*			21	*100.00*	
Location		47		26		21		0.969
	Frontal	21	*44.68*	11	*42.31*	10	*47.62*	
	Parietal	16	*34.04*	9	*34.62*	7	*33.33*	
	Temporal	2	*4.26*	1	*3.85*	1	*4.76*	
	Occipital	6	*12.77*	4	*15.38*	2	*9.52*	
	Intraventricular/extra-axial	2	*4.26*	1	*3.85*	1	*4.76*	
Tumor volume (cm^3)	Median	71.88		99.22		65.29		0.459
	Mean	126.35		154.15		86.19		
	SD	120.8		144.33		53.41		
Tumor border		45		26		19		0.274
	Well-defined (>90%)	9	*20.00*	5	*19.23*	4	*21.05*	
	Predominantly well-defined (50–90%)	29	*64.44*	15	*57.69*	14	*73.68*	
	Ill-defined (<50%)	7	*15.56*	6	*23.08*	1	*5.26*	
Edema		45		26		19		1
	No	3	*6.67*	2	*7.69*	1	*5.26*	
	Yes	42	*93.33*	24	*92.31*	18	*94.74*	
Edema width (cm)	Median	1.5		1.5		1.5		0.081
	Mean	1.72		1.55		1.95		
	SD	1.02		0.76		1.26		
Cysts		46		26		20		1
	No	4	*8.70*	2	*7.69*	2	*10.00*	
	Yes	42	*91.30*	24	*92.31*	18	*90.00*	
Predominant morphology		46		26		20		0.241
	Solid	16	*34.78*	7	*26.92*	9	*45.00*	
	Cystic	20	*43.48*	11	*42.31*	9	*45.00*	
	Central necrosis	10	*21.74*	8	*30.77*	2	*10.00*	
Peripheral cysts		46		26		20		0.681
	No	8	*17.39*	5	*19.23*	3	*15.00*	
	Yes	38	*82.61*	21	*80.77*	17	*85.00*	
Cysts signal		41		24		17		0.568
	Isointense to CSF	2	*4.88*	1	*4.17*	1	*5.88*	
	Lipid-rich (T1/T2)	23	*56.10*	12	*50.00*	11	*64.71*	
	Mixed	16	*39.02*	11	*45.83*	5	*29.41*	
Hydrocephalus		46		26		20		0.082
	No	32	*69.57*	15	*57.69*	17	*85.00*	
	Grade 1 = mild	3	*6.52*	3	*11.54*	0	*0.00*	
	Grade 2 = moderate	10	*21.74*	8	*30.77*	2	*10.00*	
	Grade 3 = severe	1	*2.17*	0	*0.00*	1	*5.00*	

Table 1 (Continued)

		RELA-fused $n=47$		Comparison *CDKN2A* WT $n=26$		*CDKN2A* del $n=21$		*p*-value
		n	%	*n*	%	*n*	%	
CE intensity		42		25		17		0.720
	None	0	*0.00*	0	*0.00*	0	*0.00*	
	Slight	1	*2.38*	1	*4.00*	0	*0.00*	
	Moderate	5	*11.90*	3	*12.00*	2	*11.76*	
	Intense	36	*85.71*	21	*84.00*	15	*88.24*	
CE homogeneity		42		25		17		0.162
	Homogeneous	1	*2.38*	0	*0.00*	1	*5.88*	
	Predominantly homogeneous	1	*2.38*	1	*4.00*	0	*0.00*	
	Predominantly inhomogeneous	4	*9.52*	4	*16.00*	0	*0.00*	
	Inhomogeneous	36	*85.71*	20	*80.00*	16	*94.12*	
CE %		42		25		17		1
	1–25%	0	*0.00*	0	*0.00*	0	*0.00*	
	25–50%	0	*0.00*	0	*0.00*	0	*0.00*	
	51–75%	0	*0.00*	0	*0.00*	0	*0.00*	
	76–100%	42	*100.00*	25	*100.00*	17	*100.00*	
T2 signal		42		26		17		0.477
	Hyperintense	2	*4.76*	2	*7.69*	0	*0.00*	
	Isointense	5	*11.90*	2	*7.69*	3	*17.65*	
	Hypointense	0	*0.00*	0	*0.00*	0	*0.00*	
	All appear	36	*85.71*	22	*84.62*	14	*82.35*	
T2 major		42		26		17		0.517
	Hyperintense	2	*4.76*	2	*7.69*	0	*0.00*	
	Isointense	40	*95.24*	24	*92.31*	17	*100.00*	
	Hypointense	0	*0.00*	0	*0.00*	0	*0.00*	
	All appear	0	*0.00*	0	*0.00*	0	*0.00*	
T2 hemorrhage		42		25		17		**0.010**
	No	11	*26.19*	4	*16.00*	7	*41.18*	
	Yes	11	*26.19*	11	*44.00*	0	*0.00*	
	Probably	20	*47.62*	10	*40.00*	10	*58.82*	
T1 Signal		41		25		16		0.654
	Hyperintense	0	*0.00*	0	*0.00*	0	*0.00*	
	Isointense	7	*17.07*	3	*12.00*	4	*25.00*	
	Hypointense	0	*0.00*	0	*0.00*	0	*0.00*	
	All appear	34	*82.93*	22	*88.00*	12	*75.00*	
T1 major		40		25		15		1
	Hyperintense	1	*2.50*	1	*4.00*	0	*0.00*	
	Isointense	39	*97.50*	24	*96.00*	15	*100.00*	
	Hypointense	0	*0.00*	0	*0.00*	0	*0.00*	
	All appear	0	*0.00*	0	*0.00*	0	*0.00*	
T1 hemorrhage		40		25		15		0.430
	No	19	*47.50*	11	*44.00*	8	*53.33*	
	Yes	13	*32.50*	10	*40.00*	3	*20.00*	
	Probably	8	*20.00*	4	*16.00*	4	*26.67*	
Tumor homogeneity (T1/T2)		43		25		18		0.758
	Homogeneous	1	*2.33*	0	*0.00*	1	*5.56*	
	Predominantly homogeneous	4	*9.30*	2	*8.00*	2	*11.11*	
	Predominantly inhomogeneous	4	*9.30*	3	*12.00*	1	*5.56*	
	Inhomogeneous	34	*79.07*	20	*80.00*	14	*77.78*	

Table 1 (Continued)

		RELA-fused $n=47$		Comparison *CDKN2A* WT $n=26$		*CDKN2A* del $n=21$		*p*-value
		n	%	*n*	%	*n*	%	
ADC		47		26		21		1
	Not available	37		18		19		
	Low values (restricted)	10	*100.00*	8	*100.00*	2	*100.00*	
	Normal or high values	0	*0.00*	0	*0.00*	0	*0.00*	
DWI		47		26		21		1
	Not available	33		15		18		
	Restricted diffusion	14	*100.00*	11	*100.00*	3	*100.00*	
	Not restricted	0	*0.00*	0	*0.00*	0	*0.00*	
SWI/T2*		47		26		21		0.390
	Not available	34		16		18		
	Blood/hemosiderin	2	*15.38*	2	*20.00*	0	*0.00*	
	Calcification	0	*0.00*	0	*0.00*	0	*0.00*	
	Differentiation not possible	8	*61.54*	6	*60.00*	2	*66.70*	
	Unremarkable	3	*23.08*	2	*20.00*	1	*33.30*	
Hemorrhage (all sequences)		45		26		19		0.068
	Yes	27	*60.00*	19	*73.08*	8	*42.11*	
	No	18	*40.00*	7	*26.92*	11	*57.89*	
CT available		47		26		21		–
	No	42	*89.36*	24	*92.31*	18	*85.71*	
	Yes	5	*10.64*	2	*7.69*	3	*14.29*	
CT: calcifications		5		2		3		0.400
	No	2	*40.00*	0	*0.00*	2	*66.70*	
	Yes	3	*60.00*	2	*100.00*	1	*33.30*	

This table shows absolute and relative (%) frequencies of patient data and MRI parameters in *RELA*-fused ST-EPN, as well as *p*-values after comparison of imaging parameters according to *CDKN2A* genomic status. Note that relative frequencies do not equal 100% in some cases, due to mathematical rounding. Statistically significant differences ($p<0.05$) are in bold print

SD standard deviation, *CE* contrast enhancement, *CT* computed tomography, *DWI* diffusion-weighted images, *ADC* apparent diffusion coefficient

distributed. For categorical variables, χ^2-test and Fisher's exact test (when two options were possible for each measurement) were conducted. To address potential error that might result from multiple testing of the dataset, Bonferroni correction was finally performed for both numerical and categorical variables. *P*-values <0.05 were considered as statistically significant and IBM (IBM Corporation, Armonk, NY, USA) SPSS for Mac (version 21) was used for all statistical analyses.

Results

Patient Population and Molecular Analysis

A total of 47 ST-EPN tested positive for *RELA* fusion (WHO grade II $n=2$, grade III $n=45$), whereas in 10 tumors the fusion protein could not be detected. The mean age of patients with *RELA*-fused ST-EPN was 7.9 ± 5.2 years (24 male, 23 female), *CDKN2A* heterozygous ($n=12$) or homozygous ($n=9$) deletions were detected in 21 cases (mean age 10.57 ± 4.78 years; 11 male, 10 female), whereas 26 cases of *RELA*-fused ST-EPN did not show *CDKN2A* deletion (mean age 5.84 ± 4.45 years; 13 male, 13 female). Examples of tumors showing nuclear RelA expression with and without p16 protein expression are shown in Supplementary Fig. S1. The patient data are summarized in Table 1.

MRI in *RELA*-fused ST-EPN

Image analysis of 47 cases showed a heterogeneous MRI morphology in *RELA*-fused ependymomas. Tumors appeared cystic (43%), solid (35%) or with central necrosis (22%). There was a pronounced morphological overlap and no clearly dominant phenotype within our cohort (typical imaging features illustrated in Fig. 1). The majority of ST-EPN were located in the frontal (45%) or parietal (34%) lobe and only 2 tumors (4%) had a solely intraventricular/extra-axial location. Tumors could be large at diagnosis (mean volume at diagnosis $=126\pm121\,cm^3$), especially when voluminous cysts were present. The presence of cysts

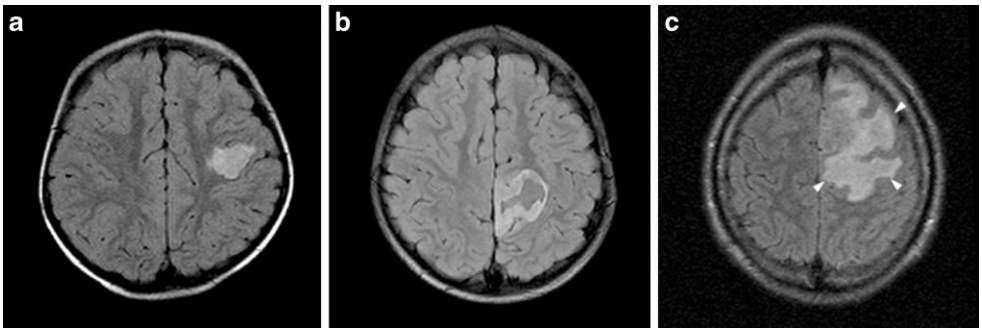

Fig. 3 Small hemispheric tumors in (**a**) (predominantly solid; Philips Intera 1.5 T) and in (**b**) (with central necrosis; Siemens Vision 1.5 T) with no relevant edema. In contrast, the small parasagittal tumor (**c**) (Siemens Harmony 1.0 T) has a marked peritumoral edema (*white arrowheads*). Note the absence of cysts. These fluid attenuated inversion recovery (FLAIR) images illustrate the morphological spectrum within *RELA*-fused ST-EPN

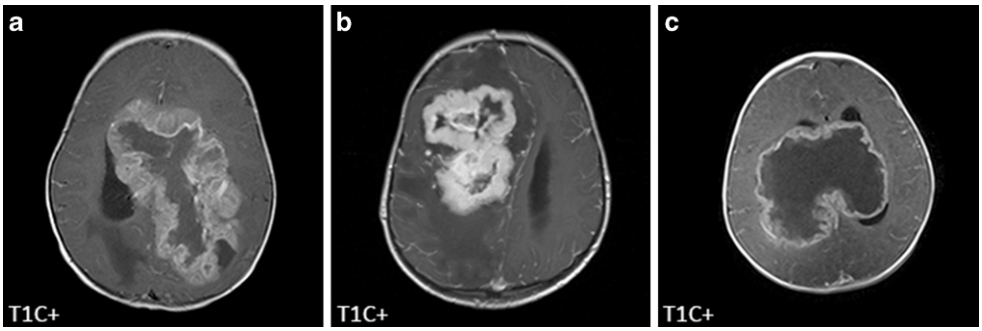

Fig. 4 Large *RELA*-fused ST-EPN with marked central necrosis and enhancing components in the periphery (**a** Philips Achieva 1.5 T; **b** Siemens Symphony 1.5 T; Siemens Harmony 1.0 T). It is of note that there might be an evolution from solid tumors across necrotic and hemorrhagic changes to cystic components during tumor growth. Note intraventricular location in (**c**)

and peritumoral edema was detected with a frequency of >90% for each category. The MRI signal (in both T1WI and T2WI) was heterogeneous in most of the cases (88%), and signs of intratumoral hemorrhage were found in 60% of cases. A DWI was available for 14 out of 47 cases, and 100% of these tumors showed a high signal (with either low signal in corresponding ADC or T2WI), suggesting diffusion restriction. All tumors showed enhancement in their solid components after intravenous gadolinium injection, with 86% showing a strong and inhomogeneous enhancement pattern. Within the 5 cases with CT scans available, calcifications could be found in 60% of the tumors. Table 1 shows a summary of the analyzed imaging parameters. The MR images of *RELA*-fused ST-EPN are shown in Figs. 1, 2, 3 and 4 and Supplementary Fig. S2.

CDKN2A Deleted Compared to CDKN2A Wild Type Tumors

Comparative analysis of *CDKN2A* deleted versus *CDKN2A* WT tumors revealed that tumors with a deletion occurred at a significantly higher age (mean 10.6 vs. 5.8 years in *CDKN2A* WT; $p = 0.02$); however, signal changes in T2WI suggestive for intratumoral hemorrhage were found more frequently in *CDKN2A* WT tumors (44% in *CDKN2A* WT vs. 0% in *CDKN2A* deleted; $p = 0.010$). All other categories were not significant. The Fig. S2 illustrates MRI findings according to *CDKN2A* genomic status.

Discussion

The use of MRI is a well-established technique for imaging evaluation of ST-EPN due to its high soft tissue contrast. Recently, neuro-oncology has begun to move beyond traditional histopathological diagnosis towards molecular stratification of brain tumors. Imaging genomics, radiogenomics, and radiomics are different terms to describe an emerging field of research focused on understanding the relationship between molecular features and medical imaging data of brain tumors [11, 12, 18]. An ST-EPN with *RELA* fusion has been defined by the 2016 WHO classification as a distinct disease entity [5]. A consensus paper recently recommended the integration of molecular-based stratification schemes in current treatment for patients with ST-EPN [13]. With respect to diagnostic imaging, it was proposed that central radiological review of presurgical and postsurgical imaging should be a principal component of every clinical trial enrolling patients with ST-EPN. This study provides

for the first time detailed data on MRI morphology of these tumors.

This cohort included 47 ST-EPN cases with NF-κB activation/*RELA* fusion (82%) that were identified in 57 patients previously diagnosed as ST-EPN, which matches with a recent publication that indicated *RELA* fusion in more than 70% of pediatric ST-EPN [19]. Pajtler et al. reported on 14/88 cases (16%) with *CDKN2A* deletion in *RELA*-fused ST-EPN, compared to 21/47 cases (45%) in our study. In this cohort 10 cases tested negative for *RELA* fusions and YAP fusions, and thus could not be assigned to a distinct molecularly defined ependymoma entity. As these tumors are ill-defined, we did not use them as a comparison group. The mean age at diagnosis was 7.1 years, which closely matches the results of the study performed by Pajtler et al. (7.3 years) [3]; however, we cannot explain the result that *CDKN2A* deletions were associated with a significantly higher manifestation age in our group.

The imaging appearance of EPN is well documented in the literature, since EPN represent the third most frequent brain neoplasm in children after pilocytic astrocytomas and medulloblastomas [20]. The ST-EPN have been described as heterogeneous tumors that may contain cysts, calcifications, and sometimes hemorrhage and after gadolinium administration, ST-EPN may demonstrate irregular, heterogeneous enhancement [21, 22]; however, ST-EPN account for 40% of all pediatric EPN, and imaging appearance of infratentorial (=posterior fossa) EPN as well as clinical and biological behavior are distinct [13, 21, 22]. Tumor location in the supratentorial compartment did not depend on *CDKN2A* deletion in our study. The majority of *RELA*-fused ST-EPN showed a frontal or parietal location. We found one case in each of the *CDKN2A* deleted and *CDKN2A* WT groups with an intraventricular/extra-axial origin (example in Fig. 4c). It is known that EPN can arise along the entire neuraxis; however, most ST-EPN are located outside the ventricles with relation to the ependymal lineage. With our data we cannot confirm findings in other brain tumor entities, such as medulloblastoma, where tumor location in the posterior fossa can be connected to specific pathway activation and to derivation from potential progenitor cells [12, 23, 24].

The heterogeneous signal in both T1WI and T2WI in *RELA*-fused ST-EPN point to an aggressive growth of this entity with intratumoral hemorrhage and necrosis. This is in accordance with our previous study that showed heterogeneous masses with cysts and hemorrhage as typical findings for EPN in a cohort with predominant supratentorial location [25]. It is important to keep in mind that necrosis can be difficult to distinguish from a tumor cyst in MRI. Especially large tumors often show central necrosis (Fig. 4) and cysts (Fig. 2c,d), whereas components merely appearing as cysts may instead develop from former necrotic parts or decomposition of intratumoral hemorrhage (Fig. 1c, S2F). For determination of tumor volume, we measured tumor diameter including cysts, with large cysts thus influencing tumor volume. We found a spectrum from small ST-EPN without cysts (Fig. 3a,c) to large predominantly cystic tumors (Fig. 2c,d). In general, the comparison of tumor size with the literature data is inaccurate, since methods for diameter measurement and volume calculation vary.

Whereas signs of intratumoral hemorrhage were frequently found, present in 60% of all *RELA*-fused ST-EPN, the statistical analysis suggests that the frequency of hemorrhage in T2WI may be related to *CDKN2A* deletion (more often in *CDKN2A* WT tumors, $p=0.001$, Fig. S2D-F). The biological background and clinical relevance of this finding can be questioned: it only refers to T2WI and could not be confirmed in other sequences or, if available, in CT. This might be due to limited availability of SWI/filtered phase images and/or respective CT scans provided by the referring centers. A reliable differentiation between hemorrhage and calcifications was challenging in some cases for the same reasons. The use of CT scans are always of help to identify calcifications; in cases where CT scans were available, we found calcifications in 60% of *RELA*-fused ST-EPN. This finding aligns with the literature, where calcifications were reported in 40–80% of EPN [25, 26].

Peritumoral edema was present in 93% of all *RELA*-fused tumors. At present, no sequences in morphological MRI exist to reliably analyze tumor infiltration. As in other brain tumor entities, there was no definite relationship between tumor volume and edema formation in our study, as we also found small tumors with impressive edema (Fig. 3c). There was furthermore no significant difference in edema formation according to *CDKN2A* deletion. The same applies for contrast enhancement, which was present (to different degrees) in all *RELA*-fused tumors and without any significant difference in enhancement pattern between *CDKN2A* deleted and *CDKN2A* WT tumors. Contrast intensity is a relatively subjective parameter and the image impression might be dependent on the MRI scanner and the scanning protocol.

In DWI, all tumors showed diffusion restriction, reflecting high cellularity (Fig. 1d); however, DWI was available for only 30% of all *RELA*-fused tumors. This is mainly due to the fact that routine protocols did not include DWI sequences in older MRI studies. Furthermore, restricted diffusion could be confirmed by low ADC (compared to normal brain) in only 71% of cases due to limited availability; however, diffusion restriction (high signal) in DWI was presumed when the corresponding T2 signal was low, even if ADC was not available. The use of DWI can be valuable in differentiating *RELA*-fused ST-EPN from other tumor entities with lower cellularity, such as low-grade astrocytoma.

The limitations of this study originate from the heterogeneous MRI dataset (from the technical point of view) with MRI scans from different manufacturers and inconsistent sequence parameters among the referring centers. In our dataset, we could not analyze advanced MRI techniques, such as MRI perfusion, MR spectroscopy, or ultrahigh field MRI, as these were not implemented in routine MRI of the referring centers. On the other hand, the multicenter approach provides us with a comparatively large study cohort with known molecular features (according to the 2016 WHO classification), and the central review of neuropathological and neuroradiological findings ensures a high level of experience and consistency. It is of note that a minor fraction of ST-EPN without *RELA* fusion has been described to carry recurrent *YAP1* (yes-associated protein 1) fusions [13]. All tumors of our cohort tested negative for *YAP1* fusion. The imaging characteristics of *YAP*-fused tumors have not yet been investigated.

In summary, we found a spectrum of MRI phenotypes in *RELA*-fused ST-EPN. Tumors can be large at diagnosis, with heterogeneous signals in T1WI and T2WI. Cysts, intratumoral hemorrhage and peritumoral edema can be frequently found. All tumors showed a certain degree of contrast enhancement, as well as diffusion restriction. The anatomical location within the supratentorial compartment also did not seem to depend on *RELA* fusion or CDKN2A deletion. Our results should be validated in a prospective cohort with defined imaging parameters.

Conclusion

This is the first detailed analysis of MR morphology in *RELA*-fused ST-EPN, with respect to *CDKN2A* genomic status. We identified imaging parameters that significantly differ in ST-EPN according to *CDKN2A* alteration. Patient stratification by means of MRI alone, however, does not seem to be feasible at present. Our results may significantly support ongoing research in ST-EPN within the framework of the radiogenomics concept.

Acknowledgements This work was supported by the German Childhood Cancer Foundation.

Conflict of interest J. Nowak, S.T. Jünger, H. Huflage, C. Seidel, A. Hohm, L.A. Vandergrift, K. von Hoff, S. Rutkowski, T. Pietsch and M. Warmuth-Metz declare that they have no competing interests.

References

1. Louis DN, Ohgaki H, Wiestler OD, Cavenee WK, Burger PC, Jouvet A, Scheithauer BW, Kleihues P. The 2007 WHO classification of tumours of the central nervous system. Acta Neuropathol. 2007;114:97–109.
2. Taylor MD, Poppleton H, Fuller C, Su X, Liu Y, Jensen P, Magdaleno S, Dalton J, Calabrese C, Board J, Macdonald T, Rutka J, Guha A, Gajjar A, Curran T, Gilbertson RJ. Radial glia cells are candidate stem cells of ependymoma. Cancer Cell. 2005;8:323–35.
3. Pajtler KW, Witt H, Sill M, Jones DT, Hovestadt V, Kratochwil F, Wani K, Tatevossian R, Punchihewa C, Johann P, Reimand J, Warnatz HJ, Ryzhova M, Mack S, Ramaswamy V, Capper D, Schweizer L, Sieber L, Wittmann A, Huang Z, van Sluis P, Volckmann R, Koster J, Versteeg R, Fults D, Toledano H, Avigad S, Hoffman LM, Donson AM, Foreman N, Hewer E, Zitterbart K, Gilbert M, Armstrong TS, Gupta N, Allen JC, Karajannis MA, Zagzag D, Hasselblatt M, Kulozik AE, Witt O Collins VP, von Hoff K, Rutkowski S, Pietsch T, Bader G, Yaspo ML, von Deimling A, Lichter P, Taylor MD, Gilbertson R, Ellison DW, Aldape K, Korshunov A, Kool M, Pfister SM. Molecular classification of ependymal tumors across all CNS compartments, histopathological grades, and age groups. Cancer Cell. 2015;27:728–43.
4. Pajtler KW, Pfister SM, Kool M. Molecular dissection of ependymomas. Oncoscience. 2015;2:827–8.
5. Louis DN, Perry A, Reifenberger G, von Deimling A, Figarella-Branger D, Cavenee WK, Ohgaki H, Wiestler OD, Kleihues P, Ellison DW. The 2016 World Health Organization classification of tumors of the central nervous system: a summary. Acta Neuropathol. 2016;131:803–20.
6. Korshunov A, Golanov A, Timirgaz V. p14ARF protein (FL-132) immunoreactivity in intracranial ependymomas and its prognostic significance: an analysis of 103 cases. Acta Neuropathol. 2001;102:271–7.
7. Korshunov A, Witt H, Hielscher T, Benner A, Remke M, Ryzhova M, Milde T, Bender S, Wittmann A, Schöttler A, Kulozik AE, Witt O, von Deimling A, Lichter P, Pfister S. Molecular staging of intracranial ependymoma in children and adults. J Clin Oncol. 2010;28:3182–90.
8. Milde T, Kleber S, Korshunov A, Witt H, Hielscher T, Koch P, Kopp HG, Jugold M, Deubzer HE, Oehme I, Lodrini M, Gröne HJ, Benner A, Brüstle O, Gilbertson RJ, von Deimling A, Kulozik AE, Pfister SM, Martin-Villalba A, Witt O. A novel human high-risk ependymoma stem cell model reveals the differentiation-inducing potential of the histone deacetylase inhibitor Vorinostat. Acta Neuropathol. 2011;122:637–50.
9. Milde T, Pfister S, Korshunov A, Deubzer HE, Oehme I, Ernst A, Starzinski-Powitz A, Seitz A, Lichter P, von Deimling A, Witt O. Stepwise accumulation of distinct genomic aberrations in a patient with progressively metastasizing ependymoma. Genes Chromosomes Cancer. 2009;48:229–38.
10. Ellingson BM. Radiogenomics and imaging phenotypes in glioblastoma: novel observations and correlation with molecular characteristics. Curr Neurol Neurosci Rep. 2015;15:506.
11. Gevaert O, Mitchell LA, Achrol AS, Xu J, Echegaray S, Steinberg GK, Cheshier SH, Napel S, Zaharchuk G, Plevritis SK. Glioblastoma multiforme: exploratory radiogenomic analysis by using quantitative image features. Radiology. 2014;273:168–74.
12. Perreault S, Ramaswamy V, Achrol AS, Chao K, Liu TT, Shih D, Remke M, Schubert S, Bouffet E, Fisher PG, Partap S, Vogel H, Taylor MD, Cho YJ, Yeom KW. MRI surrogates for molecular subgroups of medulloblastoma. AJNR Am J Neuroradiol. 2014;35:1263–9.
13. Pajtler KW, Mack SC, Ramaswamy V, Smith CA, Witt H, Smith A, Hansford JR, von Hoff K, Wright KD, Hwang E, Frappaz D, Kanemura Y, Massimino M, Faure-Conter C, Modena P, Tabori U, Warren KE, Holland EC, Ichimura K, Giangaspero F, Castel D, von Deimling A, Kool M, Dirks PB, Grundy RG, Foreman NK, Gajjar A, Korshunov A, Finlay J, Gilbertson RJ, Ellison DW, Aldape KD, Merchant TE, Bouffet E, Pfister SM3, Taylor MD. The current consensus on the clinical management of intracranial ependymoma and its distinct molecular variants. Acta Neuropathol. 2017;133:5–12.

14. Figarella-Branger D, Lechapt-Zalcman E, Tabouret E, Jünger S, de Paula AM, Bouvier C, Colin C, Jouvet A, Forest F, Andreiuolo F, Quintin-Roue I, Machet MC, Heitzmann A, Milin S, Sevestre H, Godfraind C, Labrousse F, Metellus P, Scavarda D, Pietsch T. Supratentorial clear cell ependymomas with branching capillaries demonstrate characteristic clinicopathological features and pathological activation of nuclear factor-kappaB signaling. Neuro Oncol. 2016;18:919-27.
15. Pietsch T, Wohlers I, Goschzik T, Dreschmann V, Denkhaus D, Dörner E, Rahmann S, Klein-Hitpass L. Supratentorial ependymomas of childhood carry C11orf95-RELA fusions leading to pathological activation of the NF-kappaB signaling pathway. Acta Neuropathol. 2014;127:609–11.
16. Japp AS, Gessi M, Messing-Jünger M, Denkhaus D, Zur Mühlen A, Wolff JE, Hartung S, Kordes U, Klein-Hitpass L, Pietsch T. High-resolution genomic analysis does not qualify atypical plexus papilloma as a separate entity among choroid plexus tumors. J Neuropathol Exp Neurol. 2015;74:110–20.
17. Wang Y, Cottman M, Schiffman JD. Molecular inversion probes: a novel microarray technology and its application in cancer research. Cancer Genet. 2012;205:341–55.
18. Aboian MS, Solomon DA, Felton E, Mabray MC, Villanueva-Meyer JE, Mueller S, Cha S. Imaging characteristics of pediatric diffuse midline gliomas with histone H3 K27M mutation. AJNR Am J Neuroradiol. 2017;38:795-800.
19. Parker M, Mohankumar KM, Punchihewa C, Weinlich R, Dalton JD, Li Y, Lee R, Tatevossian RG, Phoenix TN, Thiruvenkatam R, White E, Tang B, Orisme W, Gupta K, Rusch M, Chen X, Li Y, Nagahawhatte P, Hedlund E, Finkelstein D, Wu G, Shurtleff S, Easton J, Boggs K, Yergeau D, Vadodaria B, Mulder HL, Becksfort J, Gupta P, Huether R, Ma J, Song G, Gajjar A, Merchant T, Boop F, Smith AA, Ding L, Lu C, Ochoa K, Zhao D, Fulton RS, Fulton LL, Mardis ER, Wilson RK, Downing JR, Green DR, Zhang J, Ellison DW, Gilbertson RJ. C11orf95-RELA fusions drive oncogenic NF-kappaB signalling in ependymoma. Nature. 2014;506(7489):451–5.
20. Kaatsch P, Spix C. German childhood cancer registry—Annual Report 2015 (1980–2014). Mainz: Institute of Medical Biostatistics, Epidemiology and Informatics (IMBEI) at the University Medical Center of the Johannes Gutenberg University Mainz; 2015.
21. Poussaint TY. Magnetic resonance imaging of pediatric brain tumors: state of the art. Top Magn Reson Imaging. 2001;12:411–33.
22. Osborn AG. Osborn's brain: imaging, pathology, and anatomy. Salt Lake City: Amirsys; 2013. pp. 501–4.
23. Bühren J, Christoph AH, Buslei R, Albrecht S, Wiestler OD, Pietsch T. Expression of the neurotrophin receptor p75NTR in medulloblastomas is correlated with distinct histological and clinical features: evidence for a medulloblastoma subtype derived from the external granule cell layer. J Neuropathol Exp Neurol. 2000;59:229–40.
24. Massimino M, Biassoni V, Gandola L, Garrè ML, Gatta G, Giangaspero F, Poggi G, Rutkowski S. Childhood medulloblastoma. Crit Rev Oncol Hematol. 2016;105:35–51.
25. Nowak J, Seidel C, Pietsch T, Alkonyi B, Fuss TL, Friedrich C, von Hoff K, Rutkowski S, Warmuth-Metz M. Systematic comparison of MRI findings in pediatric ependymoblastoma with ependymoma and CNS primitive neuroectodermal tumor not otherwise specified. Neuro Oncol. 2015;17:1157-65.
26. Osborn AG, Daines JH, Wing SD. The evaluation of ependymal and subependymal lesions by cranial computed tomography. Radiology. 1978;127:397–401.